

J. Bartels, N. Hildebrand, M. Nawrocki, S. Kroll, M. Maas, L. Colombi Ciacchi and K. Rezwan



Effect of divalent versus monovalent cations on the MS2 retention capacity of aminofunctionalized ceramic filters

Journal Article as: peer-reviewed accepted version (Postprint)

DOI of this document* (secondary publication): 10.26092/elib/2488

Publication date of this document: 22/09/2023

* for better findability or for reliable citation

Recommended Citation (primary publication/Version of Record) incl. DOI:

Bartels, J. and Hildebrand, N. and Nawrocki, M. and Kroll, S. and Maas, M. and Colombi Ciacchi, L. and Rezwan, K.,
Effect of divalent versus monovalent cations on the MS2 retention capacity of amino-functionalized ceramic
filter,
Phys. Chem. Chem. Phys., 2018,20(16), pages 11215-11223,
The Royal Society of Chemistry, 10.1039/C8CP01607K, <http://dx.doi.org/10.1039/C8CP01607K>

Please note that the version of this document may differ from the final published version (Version of Record/primary publication) in terms of copy-editing, pagination, publication date and DOI. Please cite the version that you actually used. Before citing, you are also advised to check the publisher's website for any subsequent corrections or retractions (see also <https://retractionwatch.com/>).

This document is made available with all rights reserved.

Take down policy

If you believe that this document or any material on this site infringes copyright, please contact publizieren@suub.uni-bremen.de with full details and we will remove access to the material.

Effect of divalent *versus* monovalent cations on the MS2 retention capacity of amino-functionalized ceramic filters

J. Bartels,^{†a} N. Hildebrand,^{†bc} M. Nawrocki,^a S. Kroll,^{ad} M. Maas,^{†*ae} L. Colombi Ciacchi^{be} and K. Rezwani^{ae}

Ceramic capillary membranes conditioned for virus filtration *via* functionalization with *n*-(3-trimethoxysilylpropyl)diethylenetriamine (TPDA) are analyzed with respect to their virus retention capacity when using feed solutions based on monovalent and divalent salts (NaCl, MgCl₂). The log reduction value (LRV) by operating in dead-end mode using the model bacteriophage MS2 with a diameter of 25 nm and an IEP of 3.9 is as high as 9.6 when using feeds containing MgCl₂. In contrast, a lesser LRV of 6.4 is observed for feed solutions based on NaCl. The TPDA functionalized surface is simulated at the atomistic scale using explicit-solvent molecular dynamics in the presence of either Na⁺ or Mg²⁺ ions. Computational prediction of the binding free energy reveals that the Mg²⁺ ions remain preferentially adsorbed at the surface, whereas Na⁺ ions form a weakly bound dissolved ionic layer. The charge shielding between surface and amino groups by the adsorbed Mg²⁺ ions leads to an upright orientation of the TPDA molecules as opposed to a more tilted orientation in the presence of Na⁺ ions. The resulting better accessibility of the TPDA molecules is very likely responsible for the enhanced virus retention capacity using a feed solution with Mg²⁺ ions.

Received 12th March 2018,
Accepted 3rd April 2018

DOI: 10.1039/c8cp01607k

Introduction

Viruses are among the most challenging biological contaminations in water,^{1,2} food products³ and biopharmaceuticals.⁴ The contamination amount can be greatly reduced by selective virus filtration methods. These are also of interest for detecting and quantifying small virus concentrations⁵ or for preparing inactivated viral vaccines.⁶ Filtration and elimination of virus contaminations can be performed by ceramic capillary membranes specifically designed for virus adsorption *via* specific pore design⁷ and surface functionalization.⁸ As viruses generally present isoelectric points (IEPs) between 3.5 and 7.0,⁹ materials which provide a positive surface potential at neutral pH are suitable

for virus retention *via* adsorption.¹⁰ From a ceramics processing standpoint, a positive surface charge can be obtained *via* various methods, including coating,^{11,12} doping¹³ or chemical functionalization.^{14–17} Chemical functionalization with silanes is an especially versatile tool as it allows the covalent immobilization of specific functional groups to any oxide ceramic surface, thereby tailoring the surface chemistry for specific applications. Silanization proceeds *via* a hydrolysis–condensation reaction which can be performed in aqueous media,^{18,19} organic solvents (*e.g.* ethanol, toluene, chloroform, acetone or xylene)^{20–23} or in the vapor phase.^{24,25} Consequently, surface functionalization of ceramic materials is a broad and well-established research area²⁶ with innumerable materials and commercial products available, including a multitude of silanes with different functional groups (*e.g.* alkyl,^{27,28} amino,^{29,30} carboxyl^{–31,32} or sulphonate-groups¹⁹) and with a variety of spacer lengths.²⁶ Recent studies have demonstrated that tailoring the surface chemistry of materials shows great potential for interactions with specific viruses, proteins and other biomacromolecules.^{14,33–35} Especially amino groups, which are positively charged at neutral and acidic pH, can be used for the adsorption of negatively charged viruses.^{14–17} Despite the ubiquity of such functionalization approaches, in many cases very little is known about the precise chemical environment of the functional groups on the silanized material surface, especially considering interactions with biological

^a Advanced Ceramics, University of Bremen, Am Biologischen Garten 2, 28359 Bremen, Germany. E-mail: michael.maas@uni-bremen.de

^b Hybrid Materials Interfaces Group, Faculty of Production Engineering and Center for Environmental Research and Sustainable Technology (UFT), University of Bremen, Am Fallturm 1, 28359 Bremen, Germany

^c Faserinstitut Bremen e. V. – FIBRE, Am Biologischen Garten 2, 28359 Bremen, Germany

^d IfBB – Institute for Bioplastics and Biocomposites, Hochschule Hannover – University of Applied Sciences and Arts, Heisterbergallee 10A, 30453 Hannover, Germany

^e MAPEX Center for Materials and Processes, University of Bremen, Am Fallturm 1, 28359 Bremen, Germany

[†] These authors contributed equally to this work and are co-first authors.

entities in complex buffer systems. In early studies, researchers concluded that the addition of salts to buffer systems enhance the virus adsorption to membranes. It was shown that the presence of trivalent cations (Al^{3+}) promotes larger virus adsorption compared to divalent (Mg^{2+}) and monovalent cations (Na^+).^{36–38} Generalization of this finding was disputed by Lukasik *et al.*,³⁹ who demonstrated that the effects of salt ions depend on the filter type. They found that for different types of membranes and under different conditions, MgCl_2 promoted, inhibited or had no effect on virus adsorption. Typically, these effects may be explained by DLVO-theory in terms of the influence of the ionic strength on the double-layer interaction.^{40–44} Already at this level, monovalent and divalent ions behave quite differently; for instance the Debye length, calculated as $1/\kappa = 0.3/\sqrt{[\text{NaCl}]}$ and $1/\kappa = 0.18/\sqrt{[\text{MgCl}_2]}$, is reduced by about a factor of two for divalent ions with respect to monovalent ions.⁴⁵ Moreover, especially for divalent or trivalent ions, non-DLVO effects may dominate their behaviour in the very proximity of a solid surface.⁴⁵ Here, the adsorption of the ions at charged surface sites is strongly mediated by the mutual overlap of their hydration shells and is therefore both entropically and electrostatically driven.

In our previous work, we presented a straightforward chemical functionalization strategy for high-flux yttria-stabilized zirconia (YSZ) capillary membranes using *n*-(3-trimethoxysilylpropyl)-diethylenetriamine (TPDA), which converted the membrane surface potential from negative to positive.⁸ The non-functionalized capillary membranes showed IEPs < 3 which is similar to a silica surface due to the 3-aminopropyltriethoxysilane (APTES) which was used as dispersant during capillary production. In this procedure, APTES coats the YSZ particles in the slurry and is still present at the surface of the ceramic material after sintering. After functionalization, IEPs > 9 were achieved.⁸ The virus retention capacity using the model virus MS2 in saline buffer solution (0.02 M MgCl_2 , 0.15 M NaCl) increased from a log reduction value (LRV) of < 0.3 for the non-functionalized membrane to a value of 9.6 ± 0.3 for the amino-functionalized membrane.⁸

The aim of the present work is to investigate the effects on the virus filtration efficiency of TPDA functionalized YSZ capillary membranes in the presence of mono- and divalent salts (NaCl, MgCl_2). Based on our previous work, we have used the model bacteriophage MS2, which is a single-stranded RNA virus with a diameter of about 26 nm⁴⁶ and an IEP of 3.9,⁹ and TPDA functionalized YSZ capillary membranes with an average pore size (d_{50}) of 149 nm and an open porosity of $\sim 48\%$.⁸ MS2 is considered a relevant non-pathogenic surrogate for pathogenic viruses in aqueous media.^{47–49} The capillary membrane processing^{8,50} allows for a wet chemical functionalization without a meaningful effect on the accessible pore size. The virus retention capacities, and with that the filtration efficiencies, have been determined by virus filtration experiments in dead-end mode.

We assume that the filtration efficiency of the investigated membranes might directly depend on the accessibility of the terminal TPDA molecules, which in turn might be influenced by ion adsorption at the surface. To elucidate this effect, we

have performed advanced-sampling molecular dynamics simulations (MD) to analyze the effects on the atomistic scale and investigated the adsorption strengths and distributions of the ions at the surface. In our simulations, both the enthalpic and the entropic effects of ions and the water distributions formed at the surface and around the ions are accurately accounted for. In particular, our approach is designed to examine the orientation and accessibility of the TPDA functionalization dependent on the used ion type and correlate the results with the experimental findings.

Experimental section

Materials

All reagents were purchased from commercial sources and used without further purification.

The YSZ powder TZ-3YS-E (YSZ-90 nm, Lot. S305635P) was purchased from Krahn Chemie GmbH, Germany. 3-Aminopropyltriethoxysilane (APTES, 99%, product number 440140, Lot. SHBD4935V), hydrogen peroxide solution (purum p.a. $\geq 35\%$, product number 95299, Lot. BCBH5638V), magnesium chloride hexahydrate (MgCl_2 , product number M2670, Lot. BCBP4439V), polyvinyl alcohol (PVA, fully hydrolyzed, product number P1763, Lot. SLBC9027V), sodium chloride (NaCl, product number S7653, Lot. SZBF0350V), sulfuric acid (95–97%, product number 30743, Lot. SZBF0330V), tryptic soy agar (TSA, product number 22091, Lot. BCBR8554V), culture media tryptic soy broth (TSB, product number T8907, Lot. SLBL1497V) and *N*-(3-trimethoxysilylpropyl)diethylenetriamine (TPDA, product number 413348, Lot. MKBW1074V) were obtained from Sigma-Aldrich Chemie GmbH, Germany. The virus retention tests were performed with the bacteriophage MS2 (DSM Cat. No. 13767) and its host bacteria *E. coli* (DSM Cat. No. 5210) were used for virus propagation, both purchased from German Collection of Microorganisms and Cell Cultures (DSMZ), Germany.

Double-deionized water with an electrical resistance of 18 M Ω , which was obtained from a Synergy[®] apparatus (Millipore), was used for all experiments.

Fabrication of functionalized YSZ ceramic capillary membranes

The fabrication of functionalized YSZ capillary membranes by extrusion and wet chemical post-functionalization was performed as described in our previous studies.^{7,8,50}

In short, a ceramic slurry was prepared by milling 132 g YSZ powder (YSZ-90 nm) as ceramic material, 4 g APTES as dispersant, 20 g polyvinyl alcohol (PVA)–water solution (25 wt%) as binder and 13.5 g double-deionized water as solvent with 50 alumina grinding balls (diameter = 10 mm) in a planetary ball mill (PM400, Retsch, Haan, Germany) for 3 h at 350 rpm changing the rotation direction every 5 min. A self-made laboratory extruder equipped with a nozzle ($d = 2.0$ mm) and an integrated pin ($d = 1.0$ mm) was used to fabricate the capillaries with a speed of 50 cm min⁻¹. Afterwards, the extruded capillaries were dried for two days at RT and a humidity of about 50% and finally sintered in an oven

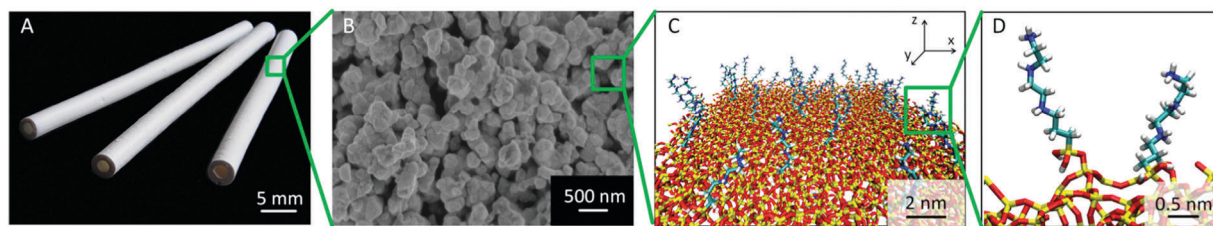


Fig. 1 Photography of TPDA functionalized zirconia tubular membrane filters (A), microstructure of the outer capillary surface (B), simulated atomistic view on a $9 \times 9 \text{ nm}^2$ part of a TPDA-functionalized surface (C) and two TPDA molecules bound to the ceramic surface (D).

(HT40/17, Nabertherm, Lilienthal, Germany) for 2 h at $1050 \text{ }^\circ\text{C}$ with dwell times at $280 \text{ }^\circ\text{C}$ (0.5 h) and $500 \text{ }^\circ\text{C}$ (1 h).

The sintered capillaries were activated by acidic hydroxylation with Piranha solution (97% H_2SO_4 :35% H_2O_2 , 3:1 (v/v)) for 30 min at RT, followed by washing with water until the effluents reached a neutral pH, and final drying at $70 \text{ }^\circ\text{C}$ for 16 h (UT6120, Heraeus, Hanau, Germany). Five capillaries with an individual length of 6 cm were incubated with 10 mL TPDA-water solution (0.2 mol L^{-1}) at $65 \text{ }^\circ\text{C}$ under slight shaking at 150 rpm (Inkubator 1000/Unimax 1010, Heidolph, Schwabach, Germany) for 24 h. Finally, the capillaries were washed until the effluents reached a neutral pH and dried at $70 \text{ }^\circ\text{C}$ for 16 h (UT6120, Heraeus, Hanau, Germany). A photography of the tubular membrane filter (A), a SEM micrograph (B), and the simulated atomistic view of the TPDA functionalized capillary membranes (C and D) are shown in Fig. 1.

Virus tests

Sterile saline solutions with different concentrations of either MgCl_2 , NaCl , or both, containing around 10^9 – 10^{10} Plaque Forming Units (PFU) per mL of MS2 bacteriophages were incubated for 2 h at RT under slight shaking at 100 rpm (Inkubator 1000/Unimax 1010, Heidolph, Schwabach, Germany). The bacteriophages were enumerated by the PFU method at the start of the incubation and after 2 h incubation time. The pH of the salt solutions was measured with a pH meter (FE20 FiveEasy, Mettler Toledo, Gießen, Germany).

The PFU method (plaque assay) which is the most quantitative and useful biological assay for viruses is based on the ability of a single virus to give rise to a macroscopic area of cytopathology on a monolayer of bacteria cells.⁵¹ Therefore, the MS2 samples were diluted in logarithmic concentration series in a salt solution (0.02 M MgCl_2 and 0.15 M NaCl). For each virus sample, three dilution series of Plaque Assays were carried out. A virus sample volume of 1.8 mL was mixed with 0.2 mL of the host bacteria and 3 mL agar and poured in a Petri dish. After an incubation time of 16 h at $37 \text{ }^\circ\text{C}$ (UN30, Memmert, Schwabach, Germany) the plaques were visible and were counted. The goal of the assay is to find the dilution of viruses that leads to the formation of countable (20–100) plaques on a Petri dish. This number is on one hand statistically significant and on the other hand individual plaques can be distinguished. Low virus dilutions (high virus concentrations) show only dead bacteria cells or too many plaques which cannot be distinguished from each other (> 100) and high virus

dilutions (low virus concentrations) have very few (< 20) or no plaques. The log reduction value (LRV) was then calculated from the counted plaques.⁵²

The virus retention test was performed as described in our previous studies,^{7,8} with slight modifications. In short, a saline solution with different concentrations of either MgCl_2 , NaCl , or both salts, containing MS2 bacteriophages in a concentration of around 10^9 – 10^{10} PFU mL^{-1} , served as viral feed solution. The virus retention test was performed in dead-end mode, which implies that one end of the capillary was sealed with silicone (Wirosil Dublier-Silikon, Bego Medical GmbH, Bremen, Germany) and the other end was connected to a peristaltic pump (BVP Standard, Ismatec, Wertheim, Germany). The feed was filtrated at an applied pressure of 500 mbar until a permeate volume of 15 mL was obtained. The pressure was determined with a manometer (C9500, Comark, Mörfelden-Walldorf, Germany). Three individual capillary membranes with an accessible length of 5 cm were tested for each salt concentration in the feed solution. The bacteriophages MS2 were enumerated using the PFU method. When no viruses (plaques) could be detected on both the diluted and the undiluted permeate sample, the LRV is calculated from the viral feed concentration. Therefore, the highest detectable LRVs are between 9 and 10 based on the feed concentration which varies between 10^9 and 10^{10} PFU mL^{-1} .

A sketch of the principle of the virus filtration test using TPDA functionalized capillaries is shown in Fig. 2.

The hydrodynamic diameter of the bacteriophage MS2 was measured *via* dynamic light scattering (Malvern Instruments, Zetasizer Nano ZSP). The results were number weighted.

Molecular dynamics simulations

The atomic structure of the amorphous silica surface ($9 \times 9 \text{ nm}^2$) is derived from Cole *et al.*⁵³ and described by the force-field MD parameters from Butenuth *et al.*⁵⁴ The primary and the two secondary amino groups of TPDA are protonated in the simulations performed at pH 6 in line with the experiment. The TPDA molecules were tethered to the surface *via* Si–O–Si bridges to deprotonated surface silanol groups, after removing the methyl groups from the Si central atom of each molecule and terminating the dangling Si–O-bonds with H atoms (see Fig. 1D).

The MD potential parameters for the TPDA molecules were taken from the AMBER GAFF force field⁵⁵ using the semi-empirical (AM1) bond charge correction (bcc) method⁵⁶ to address the molecule charges, as included in antechamber module⁵⁷ of the AMBER 14 MD simulation package.⁵⁸ We used

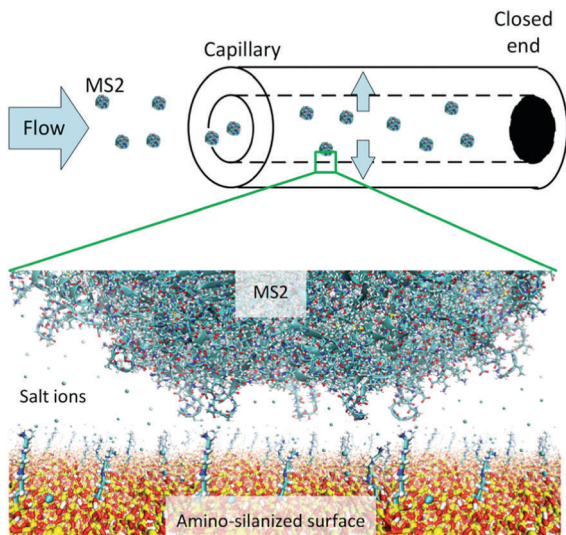


Fig. 2 Sketch illustration of the principle of dead-end filtration with ceramic capillary membranes and the bacteriophage MS2.

the default pre-set parameters to reproduce the HF/6-31G* electrostatic potential (ESP) of the molecule. Test simulations (not reported here) were performed to ensure that the resulting TPDA parameterization was fully compatible with the AMBER99SB force field. Water was described by the TIP3P model.⁵⁹ The parameters of the Na^+ and Cl^- ions were taken from the AMBER99SB force field.⁵⁸ The parameters of the Mg^{2+} ions were taken from Li *et al.*⁶⁰ The terminal silanol groups at the silica surface were protonated in accordance to pH 6 based on experimental findings as described in Hildebrand *et al.*⁶¹ All used force fields parameterizations (Butenuth, GAFF, AMBER99SB, TIP3P) are based on identical force field equations and combination rules, and thus combinable with each other.^{54,55,58}

The MD simulations were performed with the GROMACS simulation package v4.6.7, using a timestep of 2 fs.⁶² The TIP3P explicit solvent systems were carefully relaxed and equilibrated first in an *NVT* and then in a *NPT* ensemble using periodic boundary conditions. Hydrogen atoms were constrained with the LINCS algorithm.⁶³ All surface atoms except the TPDA molecules and silanol hydrogen atoms were kept fixed. The solvent density was adjusted to the TIP3P density at 1 bar and 300 K according to our previous work.⁶¹ After equilibration, the production simulations were performed in a *NVT* ensemble with a modified Berendsen thermostat with a coupling constant of 0.1 ps.⁶⁴ Long-range electrostatics was treated within periodic boundary conditions with the Smooth Particle-Mesh Ewald (SPME) method⁶⁵ using a Fourier spacing of 0.16 nm and an interpolation order of 4. A cut-off of 1.2 nm was applied for the calculation of non-bonded interaction, the neighbour-list update and the real part of the Ewald sum. Visualizations and analysis of the simulations were performed with VMD.⁶⁶

Metadynamics molecular dynamics simulations

Metadynamics simulations were performed in explicit solvent for systems including solvated ions in proximity of the silica

surface ($3 \times 3 \text{ nm}^2$), without the TPDA molecules. The distances between the ions and the deprotonated silanol groups of the surface were chosen as collective variables for well-tempered metadynamics simulations.⁶⁷ The surface contained 8 deprotonated silanol groups ($-8e$), which were partnered with either 8 Na^+ or 8 Mg^{2+} ions and 8 Cl^- ions to keep the system in each case neutral. Therefore, each system included 8 parallel metadynamics simulations. This approach is comparable to a multiple walker simulation,⁶⁸ whereas each walker has its own bias potential. A repulsive wall at distances larger than 2.5 nm built with an harmonic restraint with a force constant of $150 \text{ kJ} (\text{mol nm}^2)^{-1}$ was used to avoid interaction of the ions with the periodically repeated image of the surface slab. In addition, the ions were restrained with a weak force constant of $10 \text{ kJ} (\text{mol nm}^2)^{-1}$ in *x* and *y* directions, whereas the surface normal is oriented in *z* direction. This restraint guides the adsorption of each single ion on only one silanol group. The simulations were performed with the PLUMED v2 patch on GROMACS.^{62,69} For the well-tempered metadynamics we have used a hills width of 0.05 nm, a bias factor of 10, a tau parameter of 3 and a deposition frequency of 1 ps^{-1} .

Results and discussion

YSZ capillary membranes with a defect-free and homogeneous membrane surface were activated and silanized with TPDA, as shown in our previous study.⁸ The functionalized membranes show an average membrane pore size (d_{50}) of 149 nm combined with a relatively high open porosity of 48%, which leads to a membrane flux of $150 \text{ L} (\text{m}^2 \text{ hbar})^{-1}$ in dead-end mode.⁸ The functionalization density on the surface of the TPDA-coated capillary membranes is roughly one accessible NH_3^+ -group per nm^2 , as determined by photometrical acid-orange-II assay.⁸ The characteristic properties of TPDA functionalized ceramic capillary membranes are listed in Table 1.

Fig. 3 shows the virus retention capacity of TPDA functionalized capillaries using salt solutions with NaCl, MgCl_2 or a mixture of both salts in different concentrations. The virus retention capacity of TPDA functionalized membranes in feed solution containing 0.15 M NaCl (pH 6.3) shows a LRV of 6.5 ± 0.6 and in feed solution with 0.3 M NaCl (pH 6.3) shows a LRV of 6.2 ± 0.4 , respectively. In the presence of only divalent

Table 1 Characteristic properties of TPDA functionalized ceramic capillary membranes

Hg-porosimetry	
Pore size range	6–200 nm
d_{50}	$149 \pm 5 \text{ nm}$
Open porosity	$48.3 \pm 2.7\%$
BET method	
Specific surface area	$5.6 \pm 0.1 \text{ m}^2 \text{ g}^{-1}$
Streaming potential method	
Isoelectric point	$> 9 \text{ mV}$
Acid orange II test	
Accessible TPDA loading	$1.01 \pm 0.09 \text{ NH}_2\text{-groups per nm}^2$

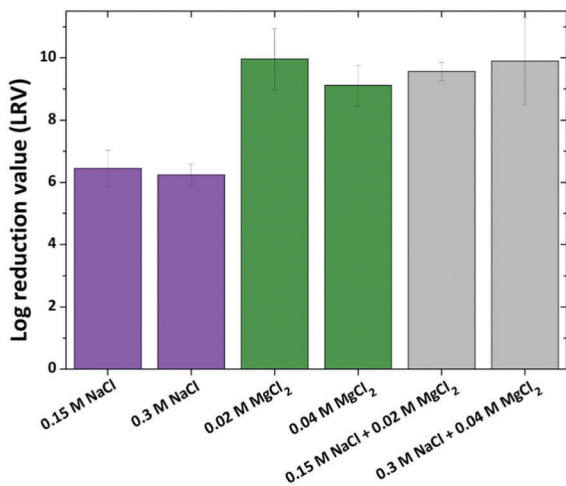


Fig. 3 Retention of the model virus MS2 mediated by TPDA functionalized capillaries using feeds based on different salt solutions (NaCl, MgCl₂ and NaCl + MgCl₂) with varying molarities and viral concentrations of $\sim 10^9$ – 10^{10} PFU mL⁻¹.

cations (Mg²⁺) in the feed solution the virus retention is increased to about 9 for both used concentrations and a nearly complete virus removal is achieved. In our previous study,⁸ a complete virus removal was obtained by filtrating the feed based on 0.15 M NaCl + 0.02 M MgCl₂ solution with 10^9 – 10^{10} PFU mL⁻¹ of MS2 phages. By comparison, the retention capacity did not significantly change when a stock solution with the same salt mixture at a different ion concentration (0.3 M NaCl + 0.04 M MgCl₂) was used. The adsorption of the virus at the filter surface occurs due to the positive membrane surface potential of TPDA functionalized capillary membranes and the overall negative surface potential of MS2 phages at the pH of 5.9. Apparently, the presence of MgCl₂ instead of (or concomitantly with) NaCl enhances the virus adsorption capability to the TPDA groups, which likely serve as the anchoring points at the ceramic surface. We can thus assume that Mg²⁺ and Na⁺ ions affect

the accessibility of the tethered TPDA molecules in different ways, leading to different virus retention properties.

To exclude any influence of the salt on the virus itself, the quantity of infectious phages in sterile saline solutions containing around 10^9 PFU mL⁻¹ of MS2 was analyzed by means of PFU tests after an incubation time of 2 h. The incubation time was chosen in accordance with the filtration time of around 1.5 h in the virus retention tests. Additionally, the colloidal stability of the virus particles was investigated *via* dynamic light scattering during this time frame. All six different salt solutions were considered. The number of MS2 phages remained stable over a time period of 2 h in all used feed solutions and no loss in activity could be observed. The number weighted hydrodynamic radius of the virus particles was constant at around 30 ± 5 nm over this time period, which indicates that the different buffers do not promote aggregation of the MS2 particles. Additionally, filtration experiments with non-functionalized capillaries (pore diameter 149 ± 5 nm) showed nearly no virus retention (LRV ~ 0.3), even in the presence of Mg²⁺. The agglomeration behaviour was also studied by Pham *et al.*⁷⁰ who measured the hydrodynamic diameter of MS2 by dynamic light scattering for Mg²⁺ concentrations between 0.1 and 1 mM. They found hydrodynamic diameters in the range between 30 and 36 nm which is slightly larger than the dimensions of each individual MS2 particle in dry state as observed with transmission electron microscopy (25–29 nm), but showed that the viruses were still monodisperse and not agglomerated. These results demonstrate that the observed virus reduction during the filtration experiment with YSZ capillaries functionalized with TPDA can be attributed to virus-membrane-feed interactions and is not significantly altered by virus inactivity or aggregation resulting from the elevated salt concentrations.

In the MD simulations we directly compare the influence of Na⁺ and Mg²⁺ ions on the orientation of the TPDA functionalization to understand the interactions of the membrane with the feed. Two systems are prepared including the positively charged TPDA molecules and negatively charged silanol groups

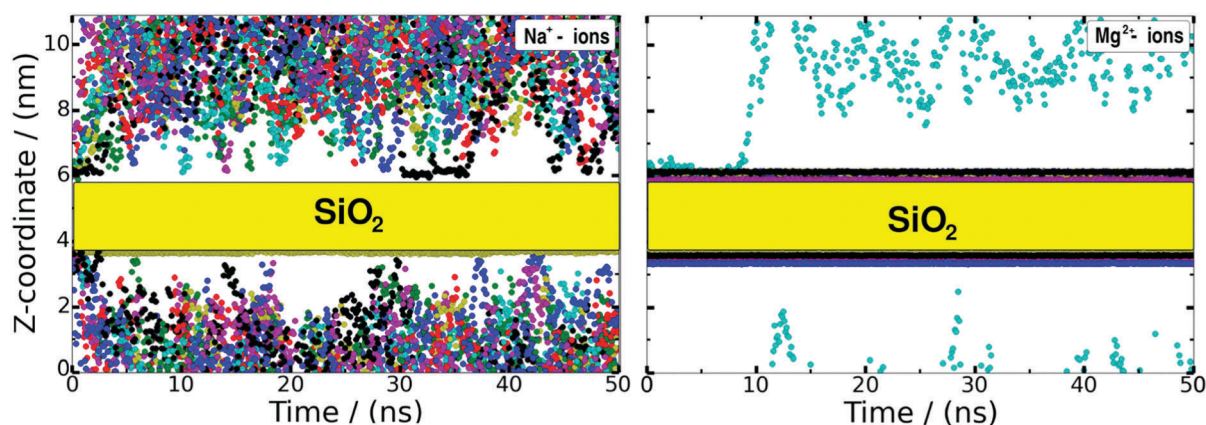


Fig. 4 Distance of the ions to the membrane surface in the surface normal direction during 50 ns all-atom explicit solvent MD simulations. The yellow bars represent the dimension of the silica surface. After initial adsorption in the start configuration, most of the Na⁺ ions (left) diffuse almost freely above the surface, whereas most of the Mg²⁺ ions (right) remain tightly adsorbed at the surface/water interface. Both systems are simulated with a concentration of the corresponding ions of 35 mM. The positions of the ions are drawn each 100 ps in a different color per ion.

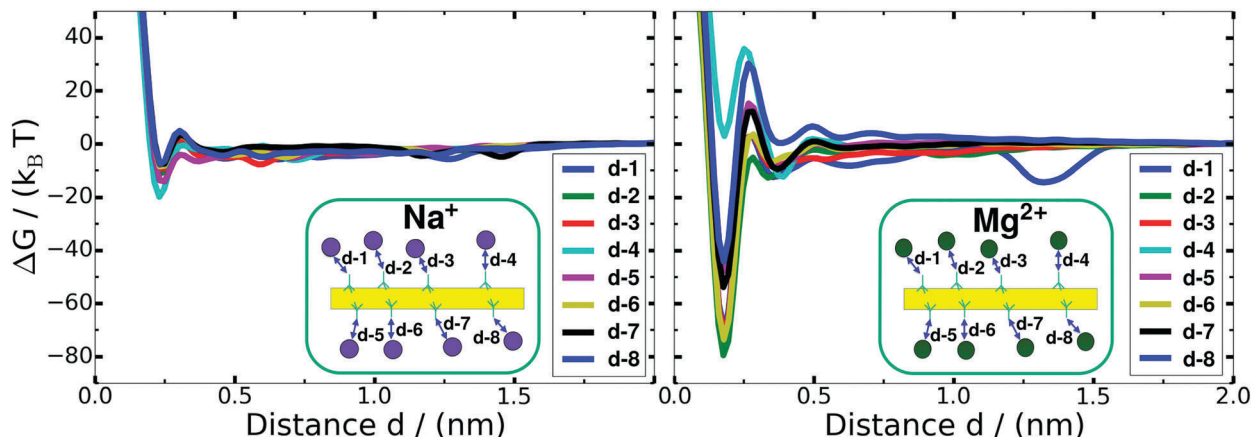


Fig. 5 Relative adsorption free energy (ΔG) profile of Na^+ (left) and Mg^{2+} ions (right) over the silanol groups of the silica surface calculated by a well-tempered metadynamics simulation using the distance to the deprotonated silanol groups as a collective variable. Eight individual metadynamics simulations are performed in one system to increase the sampling efficiency. Mg^{2+} ions show a highly increased adsorption free energy.

at pH 6, in agreement with the experiments. The surface density of TPDA molecules is adjusted to the experimental measured surface charge of about $1 e \text{ nm}^{-2}$, as measured in our recent report.⁸ Both types of ions are placed at a distance of 1.8 \AA over a deprotonated silanol group. Already within 200 ps simulation time do the Na^+ ions diffuse away from the surface towards the solvent bulk, whereas the Mg^{2+} ions remain at the deprotonated silanol surface groups for the whole simulation time of 50 ns (Fig. 4). To exclude the effect of a faster diffusion of the lighter Na^+ ions we have performed an unphysical simulation giving the Mg^{2+} ions the mass of sodium, and have found no differences in the observed dynamics.

Further, the free energy adsorption profiles of the two ions on the silanol groups of silica are computed by means of metadynamics (Fig. 5). As collective variables we have chosen the distances of each ion to the deprotonated silanol surface sites (see Methods). The obtained free energy profiles after a simulation time of 300 ns are shown in Fig. 5. A relative energy of zero is arbitrarily set to the free energy at a distance of 2.0 nm away from the oxygen atom of the silanol group. The minimum

energy basin (-11 ± 4 vs. $-54 \pm 26 k_B T$) as well as the energy barrier before adsorption (1 ± 3 vs. $12 \pm 14 k_B T$) are much stronger in the case of the Mg^{2+} with respect to the Na^+ ions, which explains why the former could not and the latter could readily desorb from the surface during the standard MD simulations (Fig. 4). We note that the strong Mg^{2+} adsorption at the surface hinders a homogeneous sampling across the collective variable, so that the presented profiles are most probably not fully converged. Nevertheless, the large difference in adsorption affinity between the two ion types is evident. The single, smaller energy basin for Mg^{2+} at a distance of 1.4 nm (shown in blue in Fig. 5) corresponds to an ion adsorbed next to a respective silanol group assigned with the distance collective variable and can be ignored. For both ion types oscillation of the free energy profiles close to the surfaces are visible, which originate from the overlap of the hydration shells of the ions and the surface's silanol groups.

The orientation of the TPDA molecules is quantitatively analyzed through calculation of both the solvent accessible surface area (SASA) and the geometric orientation of the TPDA

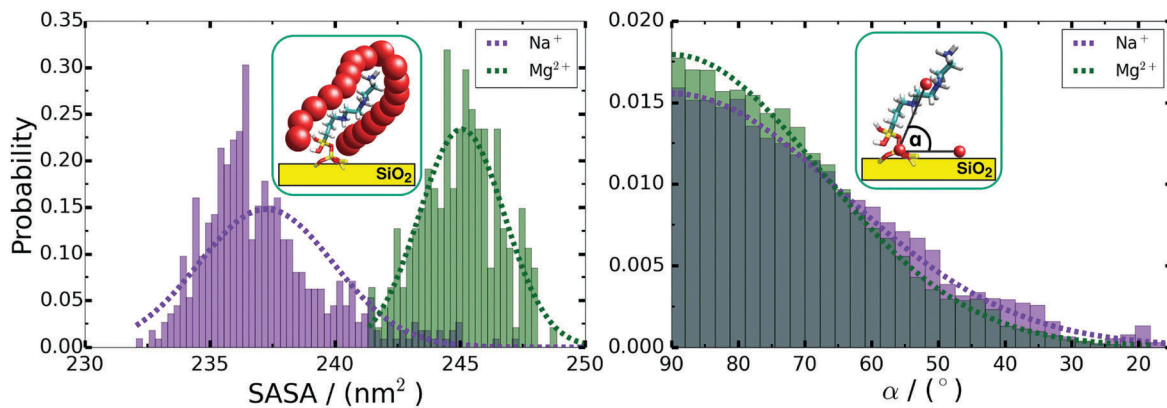


Fig. 6 Normalized histograms of the solvent accessible surface area (SASA) around the TPDA molecules using a probe radius of 1.4 \AA of the two simulated systems (left). Normalized histograms of the angle alpha between a reference molecule parallel to the surface, the central silicon atom and the center of mass of the three amino groups of the TPDA molecule. The histograms are fitted with a normal probability density function (right).

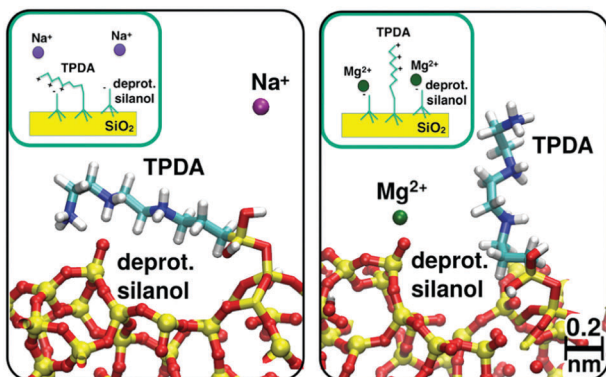


Fig. 7 Snapshots of the Molecular Dynamics (MD) simulation of two systems containing the TPDA functionalized silica surface. Deprotonated silanol groups at the surface representing a realistic pH 6 condition (left). Additional Na^+ ions are added to the system. Mg^{2+} ions replace the Na^+ ions for a direct comparison of both ion types (right).

molecule on the surface (Fig. 6) during the standard MD simulations (Fig. 4). The SASA of the functionalized surface is calculated by using a probe with a radius of 1.4 \AA in VMD.⁶⁶ A clear difference of both systems can be observed, which points towards an increased accessibility of the TPDA molecules in the case of Mg^{2+} . Furthermore, the distribution of the angle between the amino groups of TPDA and the surface along the MD trajectory (Fig. 6, right) is shifted more towards flat angles for Na^+ with respect to Mg^{2+} . This suggests that the presence of strongly adsorbed Mg^{2+} ions hinder, to a certain extent, the ionic interaction between the positive TPDA molecules and the negative, deprotonated silanol terminal groups. However, since there are many more TPDA molecules (36) than deprotonated silanols (8) on our $9 \times 9 \text{ nm}^2$ surface slab, the shift of the angle distribution is only minor, despite the larger differences of the SASA values (at pH 6). In typical trajectory snapshots, we have observed that about 5 TPDA molecules, on average, lie flat on the surface in the presence of Na^+ ions; whereas all molecules remain upright in the presence of Mg^{2+} ions.

Conclusions

In summary, our simulations suggest that different types of cations present remarkably different adsorption strengths and thus residence times on silica surfaces at neutral pH. Divalent Mg^{2+} ions effectively invert the sign of the surface potential, while Na^+ ions merely build a diffuse layer. Therefore, in the presence of only monovalent salt at low concentrations, the protonated TPDA molecules are strongly attracted by the silica surface and can assume a less accessible, rather flat orientation. When divalent cations are present (alone or in mixtures), not only is the overall surface potential more positive, but the TPDA molecules are also more upright and thus more accessible to potential binding partners, such as viruses with an overall negative surface potential (see scheme in Fig. 7). This, finally, explains why the virus retention capacity (Fig. 3) is

higher for the feed solutions which contain MgCl_2 than for the feed solution containing just NaCl .

Conflicts of interest

There are no conflicts to declare.

Acknowledgements

This work was supported by the Deutsche Forschungsgemeinschaft (DFG) under Grants KO 3811/3-1, CO 1043/4 and KR 3902/2-2. Computational resources were provided by the North-German Supercomputing-Alliance system (HLRN).

References

- 1 J. P. S. Cabral, *Int. J. Environ. Res. Public Health*, 2010, **7**, 3657–3703.
- 2 P. Reeve, R. Regel, J. Dreyfus, P. Monis, M. Lau, B. King and B. van den Akker, *Environ. Sci.: Water Res. Technol.*, 2016, **2**, 1014–1021.
- 3 M. Koopmans and E. Duizer, *Int. J. Food Microbiol.*, 2004, **90**, 23–41.
- 4 G. Miesegaes, S. Lute and K. Brorson, *Biotechnol. Bioeng.*, 2010, **106**, 238–246.
- 5 M. D. Sobsey and B. L. Jones, *Appl. Environ. Microbiol.*, 1979, **37**, 588–595.
- 6 P. Nestola, C. Peixoto, R. R. J. S. Silva, P. M. Alves, J. P. B. Mota and M. J. T. Carrondo, *Biotechnol. Bioeng.*, 2015, **112**, 843–857.
- 7 J. Werner, B. Besser, C. Brandes, S. Kroll and K. Rezwani, *J. Water Process Eng.*, 2014, **4**, 201–211.
- 8 J. Bartels, M. N. Souza, A. Schaper, P. Árki, S. Kroll and K. Rezwani, *Environ. Sci. Technol.*, 2016, **50**, 1973–1981.
- 9 B. Michen and T. Graule, *J. Appl. Microbiol.*, 2010, **109**, 388–397.
- 10 N. Kattamuri, J. H. Shin, B. Kang, C. G. Lee, J. K. Lee and C. Sung, *J. Mater. Sci.*, 2005, **40**, 4531–4539.
- 11 M. Wegmann, B. Michen, T. Luxbacher, J. Fritsch and T. Graule, *Water Res.*, 2008, **42**, 1726–1734.
- 12 M. Wegmann, B. Michen and T. Graule, *J. Eur. Ceram. Soc.*, 2008, **28**, 1603–1612.
- 13 B. Michen, J. Fritsch, C. Aneziris and T. Graule, *Environ. Sci. Technol.*, 2013, **47**, 1526–1533.
- 14 F. Meder, J. Wehling, A. Fink, B. Piel, K. Li, K. Frank, A. Rosenauer, L. Treccani, S. Koeppen, A. Dotzauer and K. Rezwani, *Biomaterials*, 2013, **34**, 4203–4213.
- 15 R. Cademartiri, H. Anany, I. Gross, R. Bhayani, M. Griffiths and M. A. Brook, *Biomaterials*, 2010, **31**, 1904–1910.
- 16 Z. Chen, F.-C. Hsu, D. Battigelli and H.-C. Chang, *Anal. Chim. Acta*, 2006, **569**, 76–82.
- 17 K. S. Zerda, C. P. Gerba, K. C. Hou and S. M. Goyal, *Appl. Environ. Microbiol.*, 1985, **49**, 91–95.
- 18 S. Kroll, C. Brandes, J. Wehling, L. Treccani, G. Grathwohl and K. Rezwani, *Environ. Sci. Technol.*, 2012, **46**, 8739–8747.

- 19 F. Meder, T. Daberkow, L. Treccani, M. Wilhelm, M. Schowalter, A. Rosenauer, L. Mädler and K. Rezwan, *Acta Biomater.*, 2012, **8**, 1221–1229.
- 20 S. Kroll, C. Soltmann, D. Koch, P. Kegler, A. Kunzmann and K. Rezwan, *Ceram. Int.*, 2014, **40**, 15763–15773.
- 21 H. J. Kim, D. H. Jung, I. H. Jung, J. I. Cifuentes, K. Y. Rhee and D. Hui, *Composites, Part B*, 2012, **43**, 1743–1748.
- 22 M. Moritz and M. Łaniecki, *Appl. Surf. Sci.*, 2012, **258**, 7523–7529.
- 23 L. A. S. A. Prado, M. Sriyai, M. Ghislandi, A. Barros-Timmons and K. Schulte, *J. Braz. Chem. Soc.*, 2010, **21**, 2238–2245.
- 24 H. Weetall, *Appl. Biochem. Biotechnol.*, 1993, **41**, 157–188.
- 25 S. Fiorilli, P. Rivolo, E. Descrovi, C. Ricciardi, L. Pasquardini, L. Lunelli, L. Vanzetti, C. Pederzoli, B. Onida and E. Garrone, *J. Colloid Interface Sci.*, 2008, **321**, 235–241.
- 26 L. Treccani, T. Y. Klein, F. Meder, K. Pardun and K. Rezwan, *Acta Biomater.*, 2013, **9**, 7115–7150.
- 27 A. Y. Ku, J. A. Ruud, T. A. Early and R. R. Corderman, *Langmuir*, 2006, **22**, 8277–8280.
- 28 J. R. Stephens, J. S. Beveridge and M. E. Williams, *Analyst*, 2011, **136**, 3797–3802.
- 29 S. Kroll, L. Treccani, K. Rezwan and G. Grathwohl, *J. Membr. Sci.*, 2010, **365**, 447–455.
- 30 J. A. Howarter and J. P. Youngblood, *Langmuir*, 2006, **22**, 11142–11147.
- 31 G. K. Toworfe, R. J. Composto, I. M. Shapiro and P. Ducheyne, *Biomaterials*, 2006, **27**, 631–642.
- 32 F. Meder, S. Kaur, L. Treccani and K. Rezwan, *Langmuir*, 2013, **29**, 12502–12510.
- 33 M. P. Calatayud, B. Sanz, V. Raffa, C. Riggio, M. R. Ibarra and G. F. Goya, *Biomaterials*, 2014, **35**, 6389–6399.
- 34 G. Hollermann, R. Dhekane, S. Kroll and K. Rezwan, *Biochem. Eng. J.*, 2017, **126**, 30–39.
- 35 P. Maffre, S. Brandholt, K. Nienhaus, L. Shang, W. J. Parak and G. U. Nienhaus, *Beilstein J. Nanotechnol.*, 2014, **5**, 2036–2047.
- 36 C. Wallis, M. Henderson and J. L. Melnick, *Appl. Microbiol.*, 1972, **23**, 476–480.
- 37 C. Wallis, J. L. Melnick and C. P. Gerba, *Annu. Rev. Microbiol.*, 1979, **33**, 413–437.
- 38 C. P. Gerba, *Adv. Appl. Microbiol.*, 1984, **30**, 133–168.
- 39 J. Lukasik, T. M. Scott, D. Andryshak and S. R. Farrah, *Appl. Environ. Microbiol.*, 2000, **66**, 2914–2920.
- 40 H. Yu, T. W. Whitfield, E. Harder, G. Lamoureux, I. Vorobyov, V. M. Anisimov, A. D. MacKerell and B. Roux, *J. Chem. Theory Comput.*, 2010, **6**, 774–786.
- 41 C. Bergonzo, K. B. Hall and T. E. Cheatham, *J. Chem. Theory Comput.*, 2016, **12**, 3382–3389.
- 42 I. C. Bourg and G. Sposito, *J. Colloid Interface Sci.*, 2011, **360**, 701–715.
- 43 H. Cao, F. T. C. Tsai and K. A. Rusch, *Groundwater*, 2010, **48**, 42–52.
- 44 S. K. Dishari, M. R. Micklin, K.-J. Sung, A. L. Zydney, A. Venkiteshwaran and J. N. Earley, *Biotechnol. Prog.*, 2015, **31**, 1280–1286.
- 45 J. N. Israelachvili, *Intermolecular and Surface Forces*, Elsevier Science, 2015.
- 46 L. Gutierrez, X. Li, J. Wang, G. Nangmenyi, J. Economy, T. B. Kuhlenschmidt, M. S. Kuhlenschmidt and T. H. Nguyen, *Water Res.*, 2009, **43**, 5198–5208.
- 47 C. Dika, C. Gantzer, A. Perrin and J. F. L. Duval, *Phys. Chem. Chem. Phys.*, 2013, **15**, 5691–5700.
- 48 N. Boudaud, C. Machinal, F. David, A. Fréval-Le Bourdonnec, J. Jossent, F. Bakanga, C. Arnal, M. P. Jaffrezic, S. Oberti and C. Gantzer, *Water Res.*, 2012, **46**, 2651–2664.
- 49 J. Langlet, L. Ogorzaly, J.-C. Schrotter, C. Machinal, F. Gaboriaud, J. F. L. Duval and C. Gantzer, *J. Membr. Sci.*, 2009, **326**, 111–116.
- 50 B. Besser, T. Veltzke, J. A. H. Dreyer, J. Bartels, M. Baune, S. Kroll, J. Thöming and K. Rezwan, *Microporous Mesoporous Mater.*, 2015, **217**, 253–261.
- 51 B. N. Fields, D. M. Knipe and P. M. Howley, *Fields' Virology*, Wolters Kluwer Health/Lippincott Williams & Wilkins, 2007.
- 52 A. Antony, J. Blackbeard and G. Leslie, *Crit. Rev. Environ. Sci. Technol.*, 2012, **42**, 891–933.
- 53 D. J. Cole, M. C. Payne, G. Csányi, S. M. Spearing and L. C. Ciacchi, *J. Chem. Phys.*, 2007, **127**, 204704.
- 54 A. Butenuth, G. Moras, J. Schneider, M. Koleini, S. Köppen, R. Meißner, L. B. Wright, T. R. Walsh and L. C. Ciacchi, *Phys. Status Solidi B*, 2012, **249**, 292–305.
- 55 J. Wang, R. M. Wolf, J. W. Caldwell, P. A. Kollman and D. A. Case, *J. Comput. Chem.*, 2004, **25**, 1157–1174.
- 56 A. Jakalian, D. B. Jack and C. I. Bayly, *J. Comput. Chem.*, 2002, **23**, 1623–1641.
- 57 J. Wang, W. Wang, P. A. Kollman and D. A. Case, *J. Mol. Graphics Modell.*, 2006, **25**, 247–260.
- 58 D. A. Case, V. Babin, J. T. Berryman, R. M. Betz, Q. Cai, D. S. Cerutti, T. E. Cheatham, T. A. Darden, R. E. Duke, H. Gohlke, A. W. Goetz, S. Gusarov, N. Homeyer, P. Janowski, J. Kaus, I. Kolossváry, A. Kovalenko, T. S. Lee, S. LeGrand, T. Luchko, R. Luo, B. Madej, K. M. Merz, F. Paesani, D. R. Roe, A. Roitberg, C. Sagui, R. Salomon-Ferrer, G. Seabra, C. L. Simmerling, W. Smith, J. Swails, R. C. Walker, J. Wang, R. M. Wolf, X. Wu and P. A. Kollman, *Amber 14*, University of California, San Francisco, 2014.
- 59 W. L. Jorgensen, J. Chandrasekhar, J. D. Madura, R. W. Impey and M. L. Klein, *J. Chem. Phys.*, 1983, **79**, 926–935.
- 60 P. Li, B. P. Roberts, D. K. Chakravorty and K. M. Merz, *J. Chem. Theory Comput.*, 2013, **9**, 2733–2748.
- 61 N. Hildebrand, S. Köppen, L. Derr, K. Li, M. Koleini, K. Rezwan and L. Colombi Ciacchi, *J. Phys. Chem. C*, 2015, **119**, 7295–7307.
- 62 S. Páll, M. J. Abraham, C. Kutzner, B. Hess and E. Lindahl, in *Solving Software Challenges for Exascale: International Conference on Exascale Applications and Software*, EASC 2014, Stockholm, Sweden, April 2–3, 2014, Revised Selected Papers, ed. S. Markidis and E. Laure, Springer International Publishing, Cham, 2015, pp. 3–27.
- 63 B. Hess, H. Bekker, H. J. C. Berendsen and J. G. E. M. Fraaije, *J. Comput. Chem.*, 1997, **18**, 1463–1472.
- 64 G. Bussi, D. Donadio and M. Parrinello, *J. Chem. Phys.*, 2007, **126**, 014101.

- 65 U. Essmann, L. Perera, M. L. Berkowitz, T. Darden, H. Lee and L. G. Pedersen, *J. Chem. Phys.*, 1995, **103**, 8577–8593.
- 66 W. Humphrey, A. Dalke and K. Schulten, *J. Mol. Graphics*, 1996, **14**, 33–38.
- 67 A. Barducci, G. Bussi and M. Parrinello, *Phys. Rev. Lett.*, 2008, **100**, 020603.
- 68 K. Minoukadeh, C. Chipot and T. Lelièvre, *J. Chem. Theory Comput.*, 2010, **6**, 1008–1017.
- 69 G. A. Tribello, M. Bonomi, D. Branduardi, C. Camilloni and G. Bussi, *Comput. Phys. Commun.*, 2014, **185**, 604–613.
- 70 M. Pham, E. A. Mintz and T. H. Nguyen, *J. Colloid Interface Sci.*, 2009, **338**, 1–9.